Figure S1

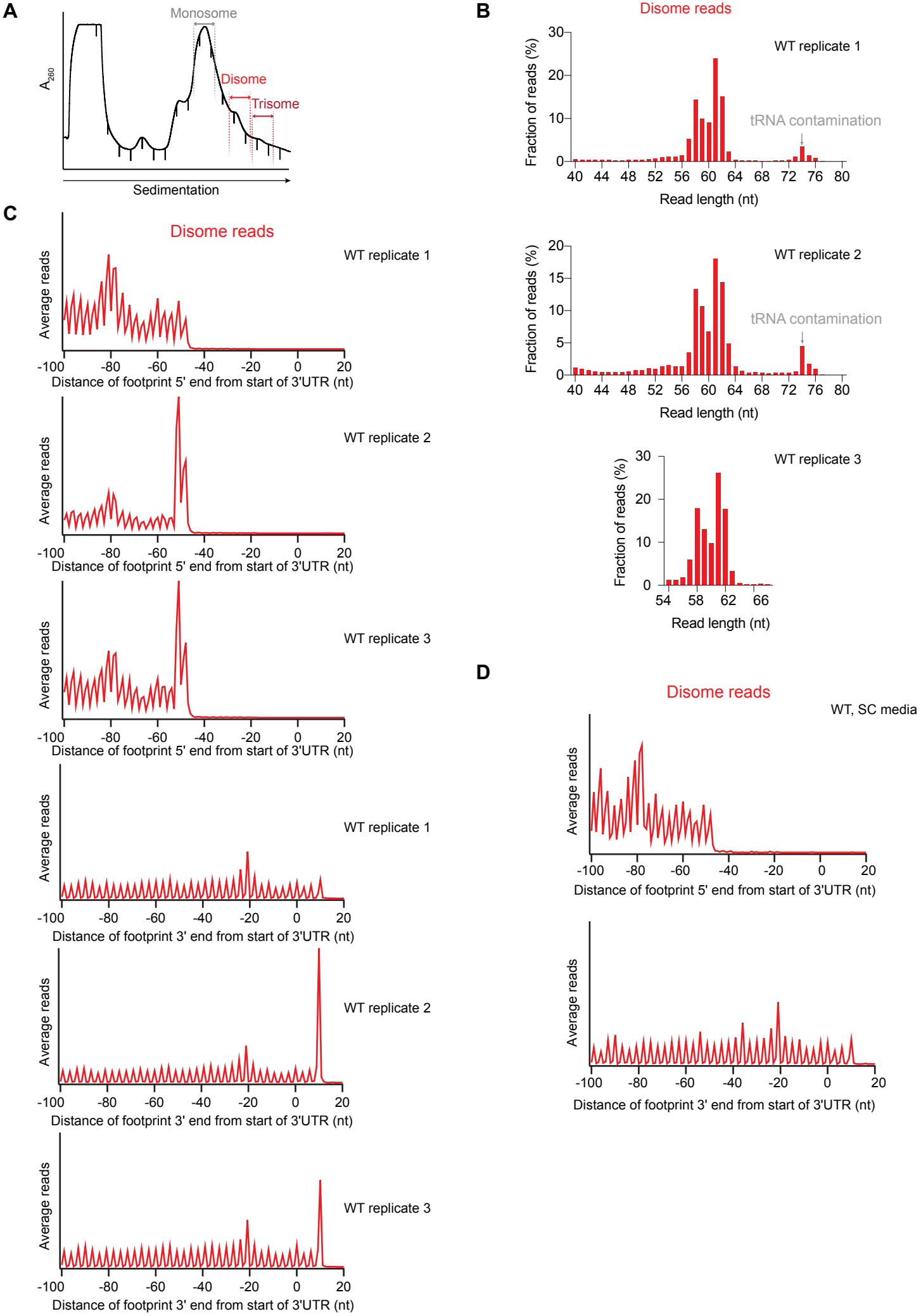
A
Monosome
Disome
Trisome
A260
Sedimentation
B
Disome reads
WT replicate 1
tRNA contamination
Fraction of reads (%)
Read length (nt)
WT replicate 2
tRNA contamination
Fraction of reads (%)
Read length (nt)
WT replicate 3
Fraction of reads (%)
Read length (nt)
C
Disome reads
WT replicate 1
Average reads
Distance of footprint 5' end from start of 3'UTR (nt)
WT replicate 2
Average reads
Distance of footprint 5' end from start of 3'UTR (nt)
WT replicate 3
Average reads
Distance of footprint 5' end from start of 3'UTR (nt)
WT replicate 1
Average reads
Distance of footprint 3' end from start of 3'UTR (nt)
WT replicate 2
Average reads
Distance of footprint 3' end from start of 3'UTR (nt)
WT replicate 3
Average reads
Distance of footprint 3' end from start of 3'UTR (nt)
D
Disome reads
WT, SC media
Average reads
Distance of footprint 5' end from start of 3'UTR (nt)
Average reads
Distance of footprint 3' end from start of 3'UTR (nt)

Figure S1: Read length distribution and metagene analysis of disome profiling replicates. Related to Figure 1.

A. An example sucrose gradient from RNase I digested WT yeast lysate. The fractions that were collected for monosome, disome and trisome profiling are indicated by dashed lines.

B. Length distribution of three replicates of disome profiling reads that are mapped to coding regions and splice junctions. Data obtained from WT cells. In all replicates, two distinct peaks at 58 and 61 nt are reproducibly observed. Note that in replicates 2 and 3, 40-80 nt mRNAs were selected during size selection, but only reads between 57 and 63 nt were used for later analysis. A peak that appears between 73-75 nt corresponds to tRNA contamination and is indicated by a gray arrow.

C. Average disome rpm mapped to ORFs that are aligned by their stop codons. Both 5' end (top) and 3' end (bottom) alignments of the footprints obtained from three replicates of WT cells are shown. Note that the presence of a stop codon peak is variable between different replicates.

D. Average disome rpm as in **C** for WT $His3^{+}$ cells grown in SC-His media are shown. The trisome profiling (Figure 1) was also performed in this strain. Note that the data obtained from cells grown in SC-His media does not substantially differ from those grown in YPD media (compare this trace to replicate 1 in **C**). In addition, growth media does not have any effect on the read length distribution (See Figure S2B, left panel).

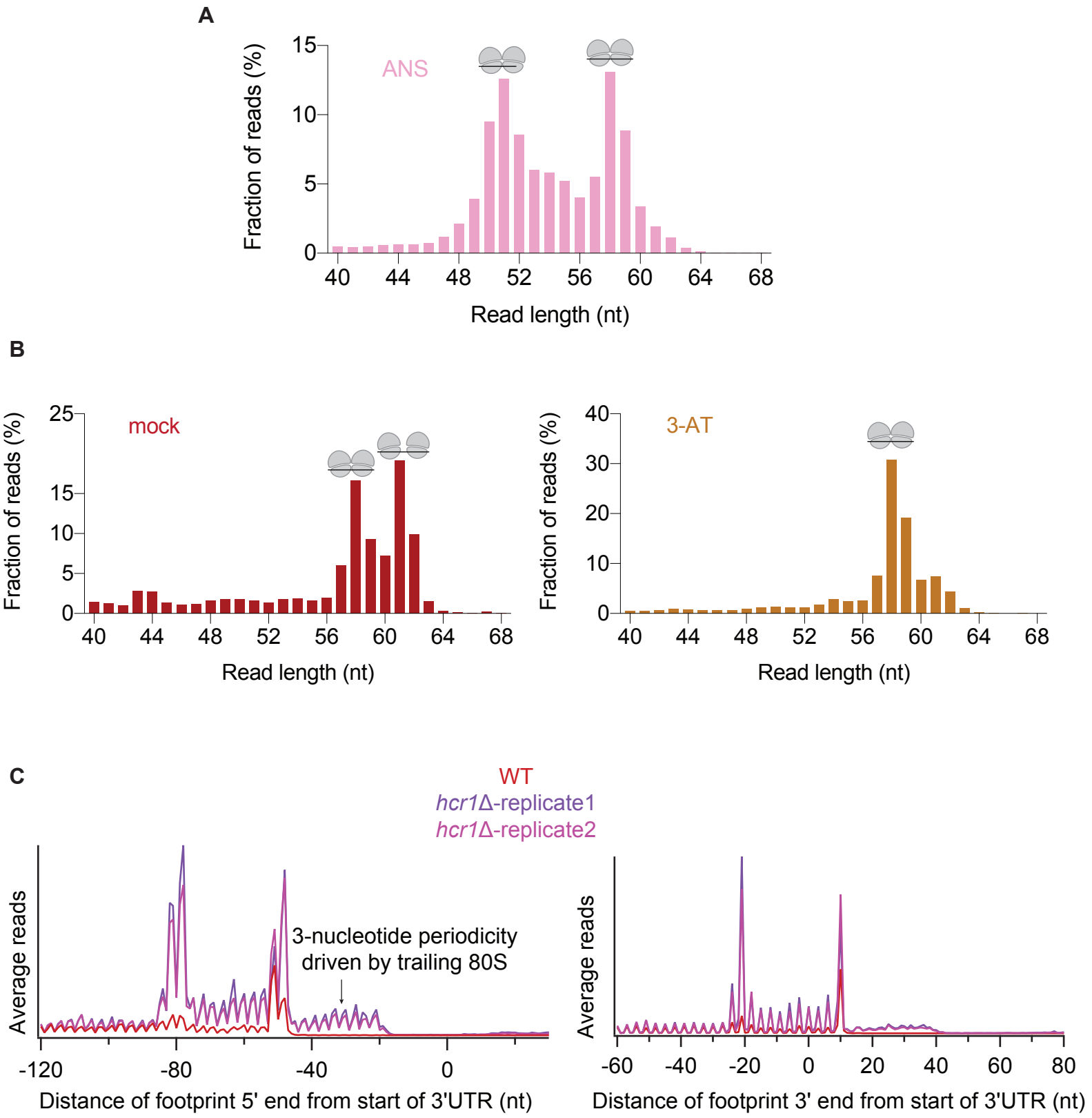
A
ANS
Fraction of reads (%)
15
10
5
0
40
44
48
52
56
60
64
68
Read length (nt)
B
mock
Fraction of reads (%)
25
15
10
5
0
Read length (nt)
3-AT
40
30
20
10
C
WT
hcr1Δ-replicate1
hcr1Δ-replicate2
Average reads
3-nucleotide periodicity
driven by trailing 80S
-120
-80
-40
0
Distance of footprint 5' end from start of 3'UTR (nt)
-60
-20
20
60
80
Distance of footprint 3' end from start of 3'UTR (nt)

Figure S2: Disome footprint size and distribution in response to various cellular stress conditions. Related to Figure 2.

A. Length distribution of disome profiling reads mapped to the coding regions and splice junctions, obtained from WT cells treated with 50 µg/mL ANS for 30 minutes prior to harvesting. Disome footprints between 40-68 nt were selected for these experiments. Note that ANS-treated cells have a distinct disome peak at 51 nt and 58 nt, presumably corresponding to compact disomes with an either open or occupied A-site, respectively.

B. Length distribution of disome profiling reads mapped to coding regions and splice junctions, obtained from mock treated cells (left) or the cells treated with 45 mM 3-AT for 30 minutes prior to harvesting. The disome footprints between 40-68 nt were selected for these experiments but we only used footprints in the range of 57-63 nt for computational analysis. 3-AT treated cells have a distinct disome peak at 58 nt, whereas the 61 nt peak is strongly diminished, consistent with a compact disome structure.

C. Average disome rpm mapped to ORFs that are aligned by their stop codons in WT (red) and *hcr1*Δ (purple) cells. 5' end (left) and 3' end (right) alignments of the footprints are shown. The 5' end alignment shows strong periodicity for the scanning disome peaks. Two biological replicates of *hcr1*Δ are shown in shades of purple.

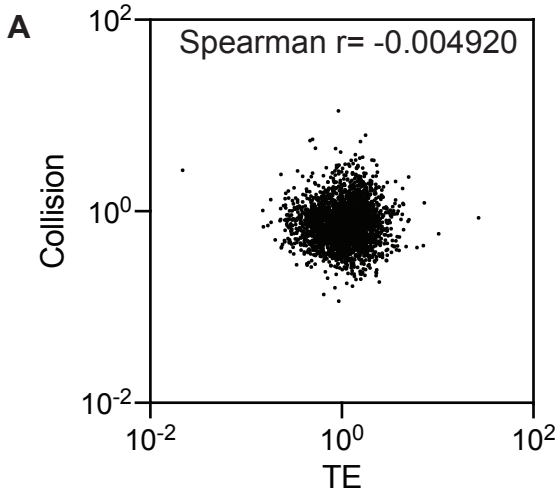
A
Spearman r= -0.004920
Collision
TE
10^2
10^0
10^{-2}

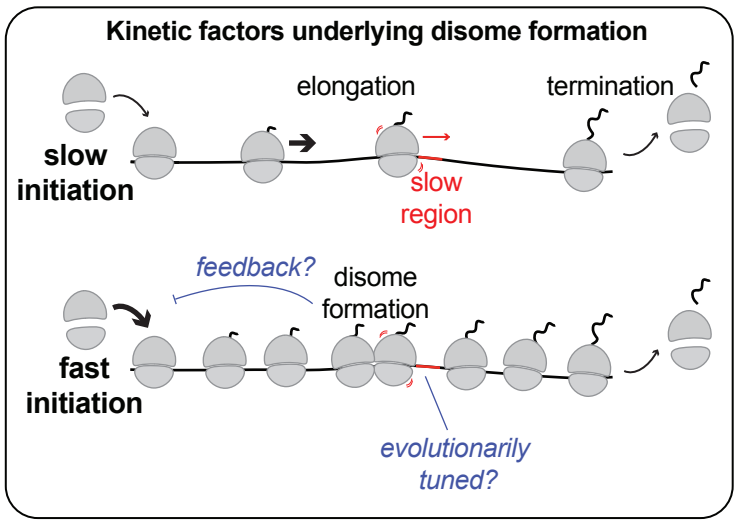
Kinetic factors underlying disome formation
elongation
termination
slow initiation
slow region
feedback?
disome formation
fast initiation
evolutionarily tuned?

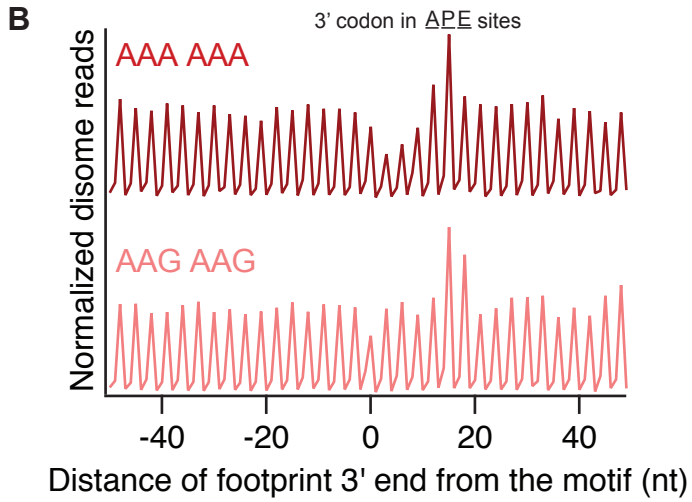
B
3' codon in APE sites
AAA AAA
AAG AAG
Normalized disome reads
-40
-20
0
20
40
Distance of footprint 3' end from the motif (nt)

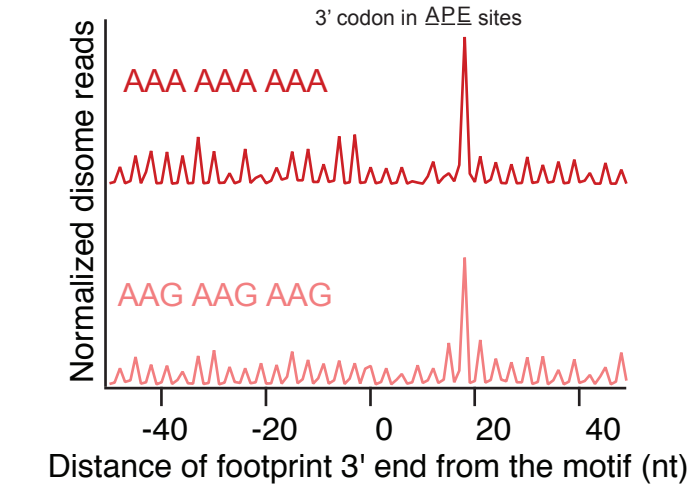
3' codon in APE sites
AAA AAA AAA
AAG AAG AAG
Normalized disome reads
-40
-20
0
20
40
Distance of footprint 3' end from the motif (nt)

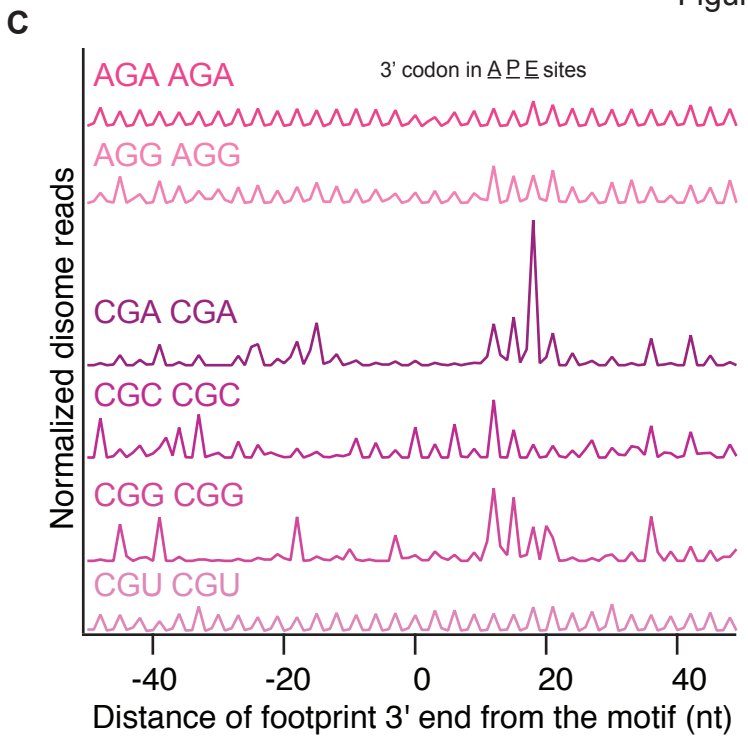
C
3' codon in APE sites
AGA AGA
AGG AGG
CGA CGA
CGC CGC
CGG CGG
CGU CGU
Normalized disome reads
-40
-20
0
20
40
Distance of footprint 3' end from the motif (nt)

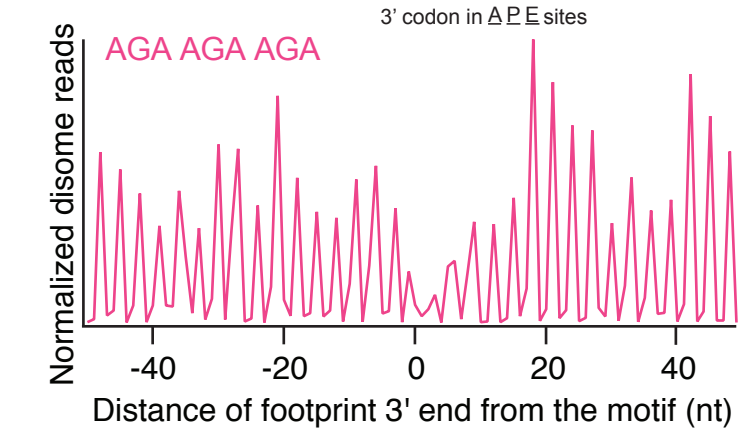
3' codon in APE sites
AGA AGA AGA
Normalized disome reads
-40
-20
0
20
40
Distance of footprint 3' end from the motif (nt)

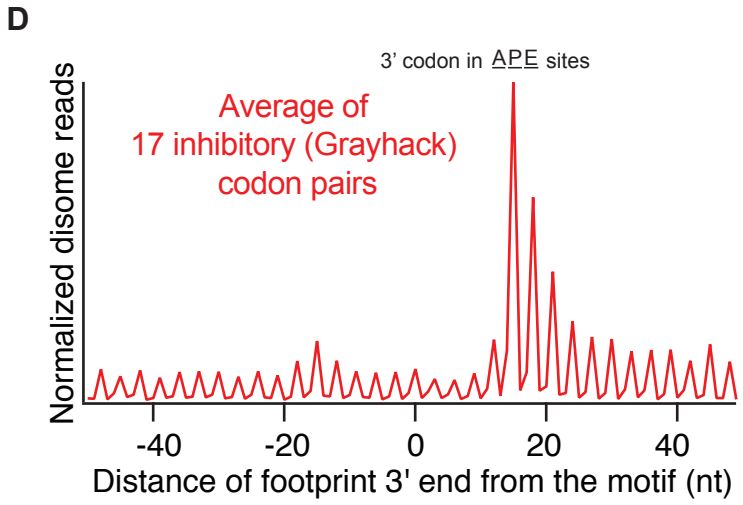
D
3' codon in APE sites
Average of
17 inhibitory (Grayhack)
codon pairs
Normalized disome reads
-40
-20
0
20
40
Distance of footprint 3' end from the motif (nt)

Figure S3: Identity of codon stretches that are enriched with disomes. Related to Figure 3.

A. Top panel: Plot comparing collision score (disome rpkm/monosome rpkm) with translation efficiency (TE, monosome rpkm/RNA-seq rpkm). Each dot represents the data for one gene with greater than 10 rpkm coverage in monosome profiling, disome profiling, and RNA-seq. The data presented here is the average of two WT biological monosome, disome and RNA-seq replicates. No correlation is observed between TE and collisions.

Bottom panel: Schematics showing how translation parameters could affect disome formation. Ribosome loading (TE) can be influenced by translation initiation, elongation and termination rates. Here, we show two different initiation rates that result in low (top) and high (bottom) TE. Rate of initiation refers to all events from 40S recruitment to the first peptidyl-transfer. Regions of slow elongation are indicated in red. We would expect that low TE leads to fewer disomes, since a stalled ribosome is less likely to collide with an upstream ribosome. In contrast, mRNAs with higher TE are expected to be more prone to disome formation. However, no correlation between TE and collisions is observed. Multiple factors that could explain the lack of correlation are indicated (blue): (1) Disome formation may directly inhibit initiation, reducing TE. (2) Slow regions may be disfavored by evolution on high TE mRNAs, reducing disome formation. See also Discussion.

B. Average disome rpm corresponding to two (top) and three (bottom) consecutive Lys codons. The reads are normalized to the total rpm within a window ±50 nt.

C. Average disome rpm corresponding to two (top) and three (bottom) consecutive Arg codons. The reads are normalized to the total rpm within a window ±50 nt. Two consecutive CGA codons exhibit the greatest disome occupancy. The number of disome reads mapping to three consecutive Arg codons was only sufficient to generate a plot in the case of AGA.

D. Average disome rpm corresponding to 17 inhibitory (Grayhack) codon pairs (CGA-CCG, CGA-GCG, CUC-CCG, CGA-CGA, CGA-AUA, CGA-CUG, CGA-CGG, CUG-CCG, GUA-CGA, CUG-CGA, GUG-CGA, AGG-CGA, AUA-CGA, GUA-CCG, AUA-CGG, CUG-AUA, AGG-CGG). The reads are normalized to the total rpm within a window ±50 nt.

For **B-D**, the positions corresponding to where the 3' codon would be for the A, P or E site of the lead ribosome is indicated above the peaks.

Figure S4

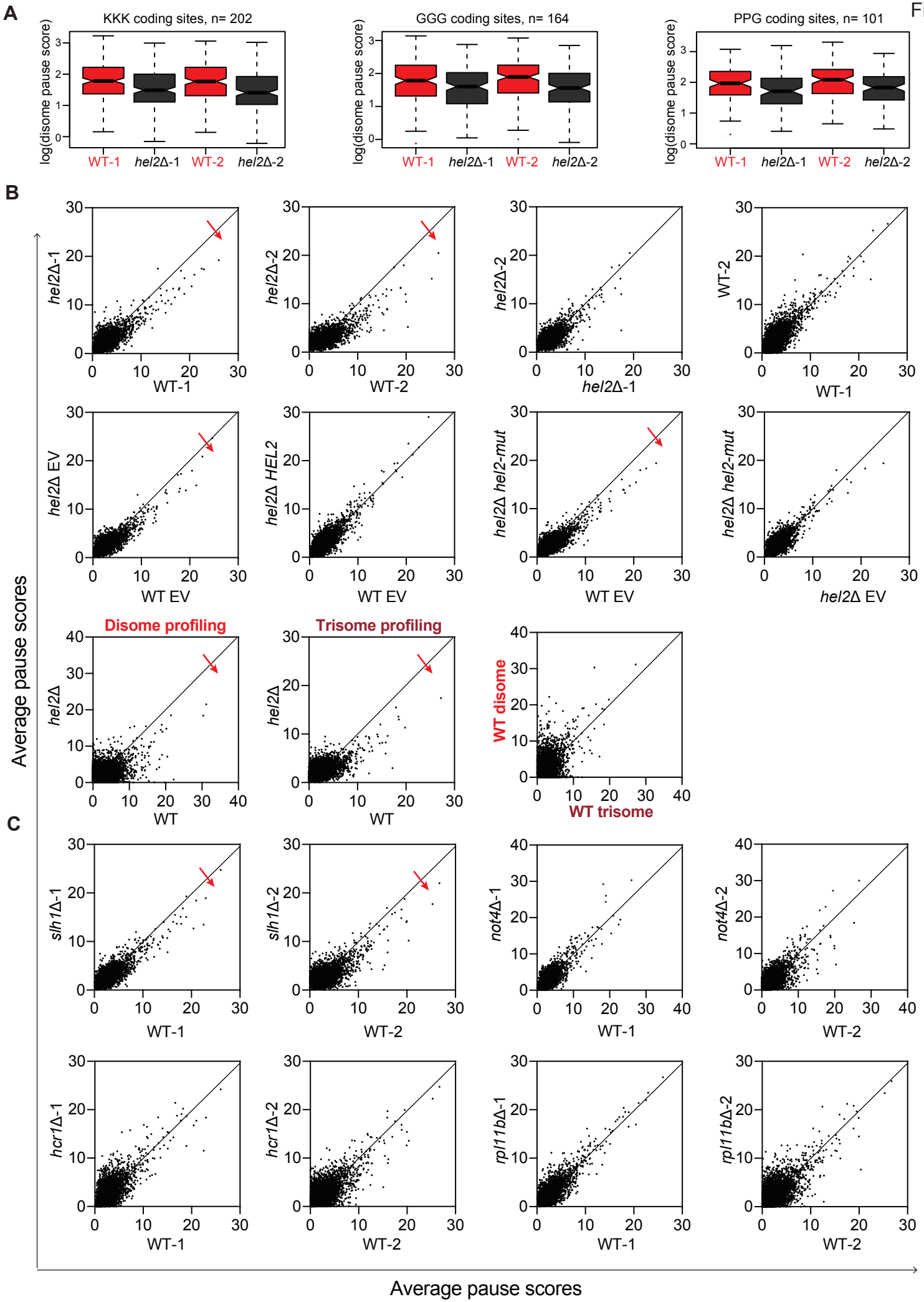
A
KKK coding sites, n= 202
GGG coding sites, n= 164
PPG coding sites, n= 101
log(disome pause score)
WT-1
hel2Δ-1
WT-2
hel2Δ-2
B
hel2Δ-1
hel2Δ-2
WT-2
hel2Δ EV
hel2Δ HEL2
hel2Δ hel2-mut
WT EV
hel2Δ EV
Disome profiling
Trisome profiling
hel2Δ
WT
WT disome
WT trisome
C
slh1Δ-1
slh1Δ-2
not4Δ-1
not4Δ-2
hcr1Δ-1
hcr1Δ-2
rpl11bΔ-1
rpl11bΔ-2
Average pause scores
Average pause scores

Figure S4: Hel2 stabilizes disomes at various motifs. Related to Figure 4.
A. Boxplots showing the distribution of disome pause scores across all KKK, GGG and PPG motifs in the transcriptome from WT (red) and *hel2*Δ (black) cells. Pause scores are calculated by dividing the rpm value at the motif by the average rpm of the window ±50 nt around the motif. Pause scores that were equal to 0 (no reads at site of interest) were eliminated from the analysis. Biological replicates for each are shown. For all comparisons, the median pause score is significantly greater in WT versus *hel2*Δ cells. Significance calculation performed on non-logged pause score values by using independent 2-group Mann Whitney U Test for each pair. p-values for each comparison: 2.4e-5 for KKK motif-replicate1, 4.4e-07 for KKK motif-replicate2; 0.0054 for GGG motif-replicate1, 3.6e-5 for GGG motif-replicate2; 0.0015 for PPG motif-replicate1, 0.00073 for PPG motif-replicate2.
B. Average disome pause scores of 6267 tripeptide motifs compared between strains. Each point in the graph represents the average score for a particular tripeptide motif. **Top row:** Average pause scores of strong stalling motifs are consistently decreased in *hel2*Δ cells, as the dots are shifted below the diagonal (shown by red arrow) in both replicates. The reproducibility of the data are shown by comparing biological replicates of each strain. **Middle row:** YCplac33 plasmids expressing WT or mutant *HEL2*, where the native promoter (P_{HEL2}) and transcription terminator (Ter_{HEL2}), from the *HEL2* ORF are used. *HEL2* expression in *hel2*Δ cells restores disome levels, as the dots are no longer shifted below the diagonal (compare the first and second graphs). Expression of an inactive Hel2 (third graph) cannot rescue disome levels and mimics the phenotype of *hel2*Δ cells (fourth graph). **Bottom row:** Disome (left) and trisome (middle) average pause scores from WT and *hel2*Δ $His3^+$ cells. Note that in both experiments, dots are shifted below the diagonal. This shows that loss of *HEL2* results in both lower disome and lower trisome accumulation for the strongest pause-inducing motifs. Comparison of WT trisome and WT disome average pause scores (right) show that the values are correlated and, therefore, trisomes are prevalent.
C. Average pause scores of the same 6267 tripeptides in **B** are compared between WT and biological replicates of many deletion strains: *slh1*Δ*, hcr1*Δ, *rpl11B*Δ and *not4*Δ. Only *slh1*Δ shows slightly similar phenotype to *hel2*Δ. Each point represents a tripeptide motif.

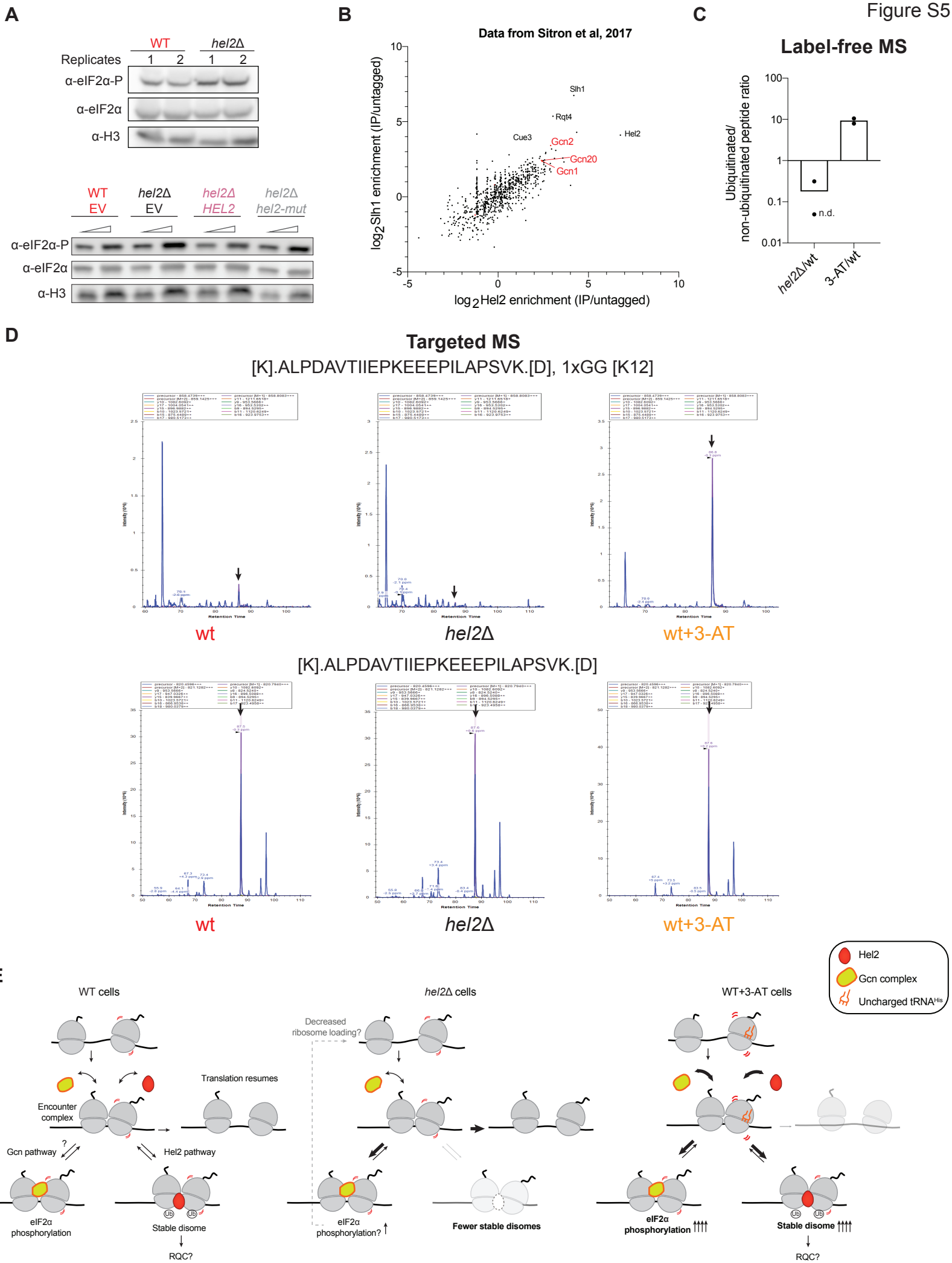
A
WT
hel2Δ
Replicates
1 2 1 2
α-eIF2α-P
α-eIF2α
α-H3
WT EV
hel2Δ EV
hel2Δ HEL2
hel2Δ hel2-mut
α-eIF2α-P
α-eIF2α
α-H3
B
Data from Sitron et al, 2017
log2Slh1 enrichment (IP/untagged)
log2Hel2 enrichment (IP/untagged)
Slh1
Rqt4
Cue3
Hel2
Gcn2
Gcn20
Gcn1
C
Label-free MS
Ubiquitinated/ non-ubiquitinated peptide ratio
n.d.
hel2Δ/wt
3-AT/wt
D
Targeted MS
[K].ALPDAVTIIEPKEEEPILAPSVK.[D], 1xGG [K12]
wt
hel2Δ
wt+3-AT
[K].ALPDAVTIIEPKEEEPILAPSVK.[D]
wt
hel2Δ
wt+3-AT
E
Hel2
Gcn complex
Uncharged tRNAHis
WT cells
hel2Δ cells
WT+3-AT cells
Encounter complex
Translation resumes
Gcn pathway
Hel2 pathway
eIF2α phosphorylation
Stable disome
RQC?
Decreased ribosome loading?
eIF2α phosphorylation?
Fewer stable disomes
eIF2α phosphorylation
Stable disome
RQC?

Figure S5: Connections between Hel2 and Gcn pathways. Related to Figure 5.

A. Top panel: Western blot showing increased eIF2α phosphorylation in *hel2*Δ compared to WT cells. Two biological replicates are shown (these are in addition to those shown in 5D). **Bottom panel:** Biological replicate of the western blot shown in Figure 5D. Note that eIF2α levels do not change in either blot. H3 (histone protein) serves as a loading control.

B. Comparison of proteins that were obtained in immunoprecipitation of Slh1 and Hel2. The data were published previously (Sitron et al, 2017). To re-create this plot, as described previously (Sitron et al, 2017), we added +1 to each spectral count value to avoid calculating the log of "0" values. Then we normalized each spectral count to total spectral counts in the respective sample. We averaged the replicates and used this average to obtain the enrichment ratio score shown on the plot. Gcn1, Gcn2 and Gcn20 are highlighted in red. Other RQT proteins, Slh1, Cue3, and Rqt4 *(YKR023W),* are also indicated on the plot.

C. Bar graph showing how uS3 ubiquitination on disomes is lowered due to loss of Hel2 but increases upon addition of 3-AT. Data obtained by label-free mass spectrometry (MS). Each dot indicates a technical replicate that is obtained from the same cellular lysate but processed independently through the sucrose gradient and MS procedure. Note that ubiquitinated uS3 was too low to be detected in one of the *hel2*Δ replicates (indicated as n.d., a value of 0.01 was automatically assigned by the MS software to avoid a "0" value). The levels of other proteins associated with disomes can be found in Supplementary Excel Tables S4 and S5.

D. Spectra from targeted MS of uS3 fragments. Sequences used for targeted MS are indicated on top of the spectra. **Top panel** shows the spectra that includes the peptide that is ubiquitinated for WT, *hel2*Δ, and WT+3-AT samples. The peak corresponding to this fragment is indicated with an arrow. Note that the intensity of this peak is ~7-fold higher in WT+3-AT compared to WT, and ~6-fold lower in h*el2*Δ sample. As an internal control for protein levels, the **bottom panel** shows that the amount of a non-ubiquitinated uS3 fragment is similar between samples.

E. Model for interaction between Gcn and Hel2 pathways. As shown Figure 4D, disomes initially form an "encounter complex" detected by sensors of ribosome collision. **Left scheme:** The Gcn complex and Hel2 both sense encounter complexes and may co-exist on sampled ribosomes. The encounter complex can trigger the Gcn pathway by activating Gcn2 and increasing levels of eIF2α phosphorylation. If the encounter complex is recognized by Hel2, collisions are stabilized and may then either be targeted to downstream RQC steps or resolve through resumed translation. **Middle scheme:** In the absence of Hel2, encounter complexes are more available to be recognized by the Gcn pathway, leading to increased eIF2α phosphorylation. Without stabilization by ubiquitin, disomes more frequently resume translation. An alternative model, which posits that ISR activation in the absence of Hel2 reduces ribosome loading on mRNAs and leads to decreased disome formation, is also indicated. **Right scheme:** His starvation induced by 3-AT increases the abundance of encounter complexes at His codons. These complexes are recognized by both Hel2 and Gcn pathways, leading to disome ubiquitination and increased eIF2α phosphorylation, respectively.

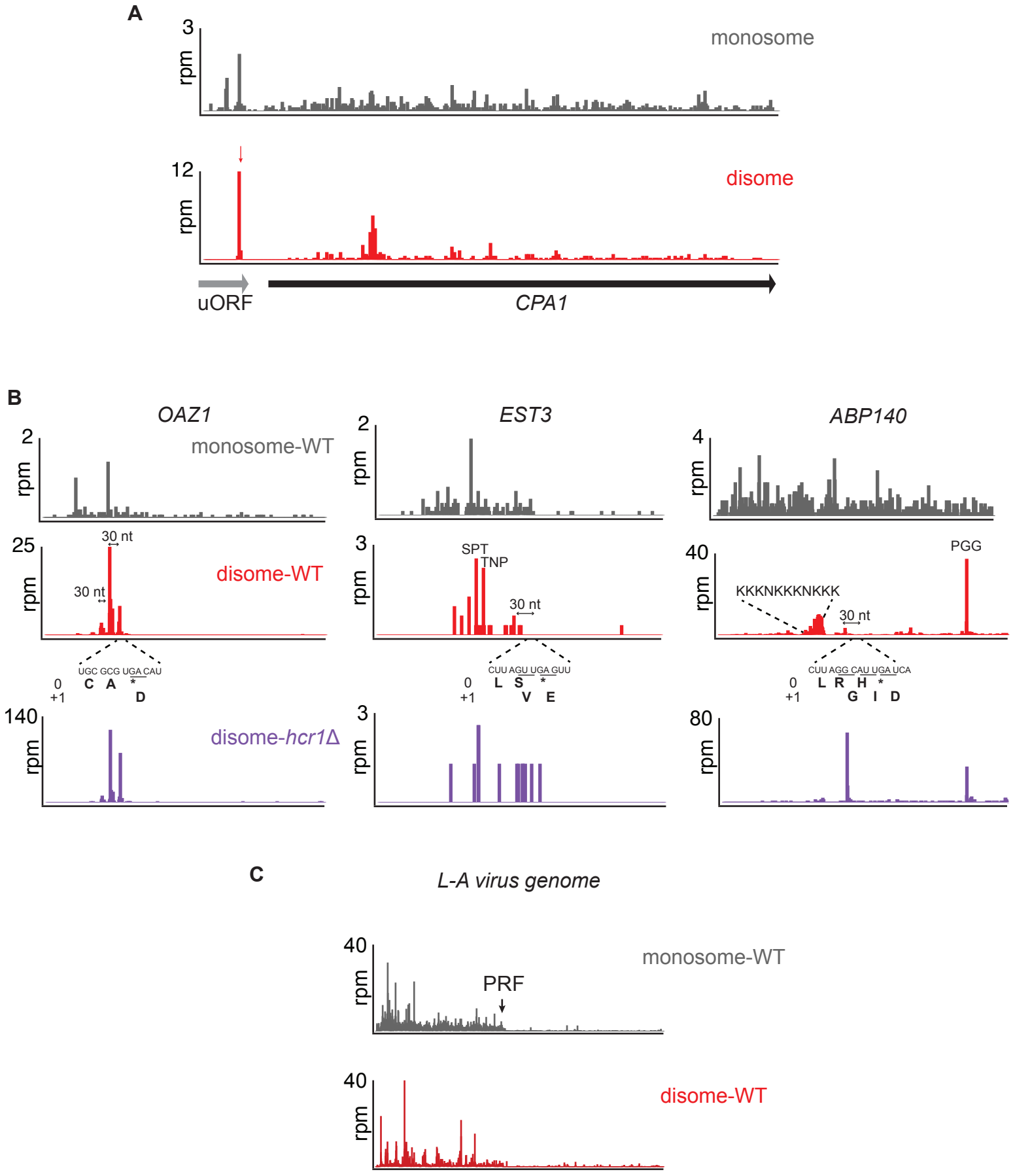
A
3
rpm
monosome
12
rpm
disome
uORF
CPA1
B
OAZ1
EST3
ABP140
2
rpm
monosome-WT
2
rpm
4
rpm
25
rpm
30 nt
30 nt
disome-WT
UGC GCG UGA CAU
0
+1
C A *
D
3
rpm
SPT
TNP
30 nt
CUU AGU UGA GUU
0
+1
L S *
V E
40
rpm
PGG
KKKNKKKNKKK
30 nt
CUU AGG CAU UGA UCA
0
+1
L R H *
G I D
140
rpm
disome-hcr1Δ
3
rpm
80
rpm
C
L-A virus genome
40
rpm
PRF
monosome-WT
40
rpm
disome-WT

Figure S6: Disomes may have functional roles in translation. Related to Figure 6.

A. Monosome (gray, top) and disome (red, bottom) footprints that map to the *CPA1* gene. Data are from pooled replicates. A disome forms due to a regulatory stalling event encoded by the *CPA1* upstream ORF (red arrow).

B. Monosome (gray, top), disome (red for WT and purple for *hcr1*Δ, bottom) footprints mapping to three cellular +1 programmed frameshifting cases. Data obtained from pooled replicates. The sequence of the frameshifting site is shown for each case and +1 and 0 frame amino acid sequences are indicated. Note that only *OAZ1* has a disome mapping to the frameshifting site, whereas *EST3* and *ABP140* show the disome upstream of the frameshifting region, which could result from queued ribosomes. Sequences that appear to trigger additional disome peaks are indicated above their respective peaks.

C. Monosome (gray, top) and disome (red, bottom) profiles of the L-A virus genome. Reads were mapped to the L-A virus genome (NC_003745.1) using Bowtie 1.1.2. -1 PRF site is indicated with an arrow. Note that a substantial disome peak around -1 PRF site does not exist.

Table S1. Yeast strains used in this study, related to STAR Methods.

Yeast name	Genotype	Source
BY4741 WT	*MATa his3Δ1 leu2Δ0 met15Δ0 ura3Δ0*	Dharmacon
BY4741 *hel2*Δ	*MATa his3Δ1 leu2Δ0 met15Δ0 ura3Δ0 hel2::KanMX4*	Dharmacon
BY4741 WT, $His3^+$ (For -/+ 3-AT disome and trisome experiments)	*MATa leu2Δ0 met15Δ0 ura3Δ0*	This study
BY4741 *hel2*Δ, $His3^+$ (For disome/trisome experiments)	*MATa leu2Δ0 met15Δ0 ura3Δ0 hel2::KanMX4*	This study
BY4741 *not4*Δ	*MATa his3Δ1 leu2Δ0 met15Δ0 ura3Δ0 not4::KanMX4*	Dharmacon
BY4741 *rpl11B*Δ	*MATa his3Δ1 leu2Δ0 met15Δ0 ura3Δ0 rpl11B::KanMX4*	Dharmacon
BY4741 *slh1*Δ	*MATa his3Δ1 leu2Δ0 met15Δ0 ura3Δ0 slh1::KanMX4*	Dharmacon
BY4741 *hcr1*Δ	*MATa his3Δ1 leu2Δ0 met15Δ0 ura3Δ0 hcr1::KanMX4*	Dharmacon

Table S2. Oligonucleotides used in this study. Related to STAR Methods.

Name	Sequence (5' to 3')
Primers that were used to construct BY4741 WT His3^{+} strain	
His3-Fwd	GAGCAGGCAAGATAAACGAAGGCAAAGATG
His3-Rev	GTATATATATCGTATGCTGCAGCTTTAAATAATCG
Primers that were used to confirm BY4741 WT His3^{+} strain for *HIS3* gene knock-in	
His3-Upstr-Fwd	AGTGCATTGGTGACTTACACATAGA
His3-Downstr-Rev	GCTCAGTTCAGCCATAATATGAAAT
Primers that were used to generate YCplac33-*HEL2* plasmid	
hel2-upstr486_Fwd	AACAGCTATGACCATGATTACGCCAAGCTTATGTAGAAGCAAGAGTACAATTCAGG
hel2-downstr256_Rev	CGACGTTGTAAAACGACGGCCAGTGAATTCAGGAACTAATCAATAATTTGACTACTCTT
Site directed mutagenesis primers that were used to generate YCplac33-*hel2-mut* plasmid	
hel2_C64AC67A_Fwd	AATTGCTGCGCGCAAGTTAACATAC
hel2_C64AC67A_Rev	ACAGCTAATTCATTTTCTTCATCAGTATCATC
RNA size selection markers	
25mer	rArUrGrUrArCrArCrGrGrArGrUrCrGrArGrCrArCrCrCrGrCrA
34mer	rArUrGrUrArCrArCrGrGrArGrUrCrGrArGrCrArCrCrCrGrCrArArCrGrCrGrArArUrG
40mer	rArUrGrUrArCrArCrGrGrArGrUrCrGrArGrCrArCrCrCrGrCrArArCrGrCrGrArArUrGrUrArCrArCrG
54mer	rArUrGrUrArCrArCrGrGrArGrUrCrGrArGrCrArCrCrCrGrCrArArCrGrCrGrArArUrGrUrArCrArCrGrGrArGrUrCrGrArGrCrArCrCrCrG
68mer	rArUrGrUrArCrArCrGrGrArGrUrCrGrArGrCrArCrCrCrGrCrArArCrGrCrGrArArUrGrUrArCrArCrGrGrArGrUrCrGrArGrCrArCrCrCrGrCrArArCrGrCrGrArUrGrUrArCrA
80mer	rArUrGrUrArCrArCrGrGrArGrUrCrGrArGrCrArCrCrCrGrCrArArCrGrCrGrArArUrGrUrArCrArCrGrGrArGrUrCrGrArGrCrArCrCrCrGrCrArArCrGrCrGrArUrGrUrArCrArCrCrCrGrCrArArCrGrCrGrA
rRNA substraction oligonucleotides	
1b	/5BioTinTEG/GGTGCACAATCGACCGATC
2b	/5BioTinTEG/GTTTCTTTACTTATTCAATGAAGCGG
3b	/5BioTinTEG/TATAGATGGATACGAATAAGGCGTC
4	/5BioTinTEG/TTGTGGCGTCGCTGAACCATAG
5	/5BioTinTEG/CAGGGGGCATGCCTGTTTGAGCGTCAT
6	/5BioTinTEG/CGGTGCCCGAGTTGTAATTT
Linker oligonucleotides	

NI-810	5´-/5Phos/NNNNNATCGTAGATCGGAAGAGCACACGTCTGAA/3ddC/
NI-811	5´-/5Phos/NNNNNAGCTAAGATCGGAAGAGCACACGTCTGAA/3ddC/
NI-812	5´-/5Phos/NNNNNCGTAAAGATCGGAAGAGCACACGTCTGAA/3ddC/
NI-813	5´-/5Phos/NNNNNCTAGAAGATCGGAAGAGCACACGTCTGAA/3ddC/
NI-814	5´-/5Phos/NNNNNGATCAAGATCGGAAGAGCACACGTCTGAA/3ddC/
NI-815	5´-/5Phos/NNNNNGCATAAGATCGGAAGAGCACACGTCTGAA/3ddC/
RT primer	
NI-802	5´- /5Phos/NNAGATCGGAAGAGCGTCGTGTAGGGAAAGAG/iSp18/GTGACTGGAG TTCAGACGTGTGCTC
PCR primers	
NI-NI-798	5´- AATGATACGGCGACCACCGAGATCTACACTCTTTCCCTACACGACGCTC
NI-799	5´- CAAGCAGAAGACGGCATACGAGATCGTGATGTGACTGGAGTTCAGACGTGT G

Table S3. Ribosome profiling statistics. Related to STAR Methods.

Sample name	Description	Data type	Reads with linker	Not aligned to non-coding RNA	Reads without PCR duplicates	Aligned to coding regions and splice junctions
SM015F	WT_rep1	Ribo-seq	32,634,770	9,956,385	8,022,682	6,435,058
SM016F	*hel2*Δ_rep1	Ribo-seq	59,462,147	15,263,501	12,283,248	10,085,580
SM023F	WT_rep2	Ribo-seq	35,194,988	12,817,968	10,280,446	8,486,785
SM024F	*hel2*Δ_rep2	Ribo-seq	42,907,002	13,731,922	11,032,308	9,122,829
SM015Fd	WT_rep1	Disome-seq	441,031,439	33,875,061	18,686,469	3,135,609
SM016Fd	*hel2*Δ_rep1	Disome-seq	211,362,149	13,897,689	8,582,714	1,677,549
SM023Fd	WT_rep2	Disome-seq	67,913,789	6,168,719	3,482,544	859,613
SM024Fd	*hel2*Δ_rep2	Disome-seq	82,170,337	10,524,816	7,606,696	3,926,150
SM025Fd	*slh1*Δ _rep1	Disome-seq	109,879,478	10,846,503	6,539,078	2,337,432
SM029Fd	*slh1*Δ_rep2	Disome-seq	114,705,670	2,931,501	2,487,287	1,139,848
SM026Fd	WT_rep3	Disome-seq	184,934,998	5,440,085	4,579,797	2,134,850
SM030Fd	*not4*Δ _rep1	Disome-seq	150,841,702	5,289,408	4,376,566	2,128,395
SM031Fd	*not4*Δ_rep2	Disome-seq	119,507,286	3,991,422	3,402,667	1,464,357
SM032Fd	*hcr1*Δ _rep1	Disome-seq	113,682,835	2,127,465	1,893,959	325,900
SM033Fd	*hcr1*Δ_rep2	Disome-seq	128,983,396	2,399,097	2,157,956	444,663
SM034Fd	*rpl11B*Δ _rep1	Disome-seq	190,193,094	4,434,485	3,888,816	842,846
SM035Fd	*rpl11B*Δ_rep2	Disome-seq	66,233,613	1,255,595	1,142,679	258,376
SM036Fd	WT_His3^{+}	Disome-seq	88,727,575	1,559,864	1,131,322	111,567
SM037Fd	WT_His3^{+}_3-AT	Disome-seq	77,677,380	1,997,656	1,618,405	561,333

SM038Fd	*hel2*Δ_ His3^{+}	Disome-seq	119,603,326	2,586,829	1,864,214	260,642
SM040Fd	WT_ANS	Disome-seq	138,642,768	5,335,853	4,285,855	2,150,720
SM042Fd	WT YCplac33	Disome-seq	47,733,375	25,415,832	5,956,757	3,967,513
SM043Fd	*hel2*Δ YCplac33	Disome-seq	43,071,227	27,558,579	5,156,939	3,450,261
SM044Fd	*hel2*Δ YCplac33-*HEL2*	Disome-seq	44,030,912	19,678,977	4,620,671	2,732,398
SM045Fd	*hel2*Δ YCplac33-*hel2-C64AC67A*	Disome-seq	40,531,321	21,847,970	4,928,916	3,414,472
SM036Ft	WT_His3^{+}	Trisome-seq	68,435,251	20,343,248	2,426,221	540,369
SM038Ft	*hel2*Δ_His3^{+}	Trisome-seq	69,672,848	35,008,524	4,334,680	2,150,045
SM015M	WT_rep1	RNA-seq	28,248,177	21,702,935	N/A	15,411,776
SM016M	*hel2*Δ_rep1	RNA-seq	60,557,306	43,444,522	N/A	27,241,161
SM023M	WT_rep2	RNA-seq	39,286,158	29,116,230	N/A	17,283,716
SM024M	*hel2*Δ_rep2	RNA-seq	51,675,601	35,070,369	N/A	16,568,700